Supporting Information

Electroreduction of CO_2 and nitrate for urea synthesis on a low-coordinated copper catalyst

Peng Guo [1], Xindong Wang [1], Yufei Wang [2], Yanwei Luo [2*], Ke Chu [3*]

[1] *School of Physics and Optoelectronic Engineering, Zhongyuan University of Technology, Zhengzhou 451191, China*

[2] *School of Physics, Henan University of Technology, Zhengzhou 450001, China*

[3] *School of Materials Science and Engineering, Lanzhou Jiaotong University, Lanzhou 730070, China*

*Corresponding author. E-mail: luoyanwei@haut.edu.cn (Y. Luo), chuk630@mail.lzjtu.cn (K. Chu)

Experimental Section

Materials

$Cu(CH_3COO)_2·H_2O$ (≥99.0%), $NaNO_2$ (≥99.0%), $C_6H_5Na_3O_7·2H_2O$ (≥99.0%), $C_5FeN_6Na_2O·2H_2O$ (≥99.0%) and NaClO (≥99.9%), $C_7H_6O_3$ (≥99.5%), NH_4Cl (≥99.5%), urease, N_2H_4 (≥99.0%), $NaNO_2$ (≥99.9%) and Nafion (5 wt%) were provided from Sigma–Aldrich Chemical Reagent Co., Ltd. CO_2 (≥99.999%) and Ar (≥99.999%) are provided from Lanzhou Xinwanke, Co., Ltd. All reagents were analytical reagent grade without further purification.

Synthesis of Cu

Pristine Cu was synthesized through a spray pyrolysis strategy. Briefly, a precursor solution was prepared by dissolving 6.0 g of $Cu(CH_3COO)_2·H_2O$ in 3.0 L of deionized water. The precursor solution was atomized using a homemade ultrasonic atomizer with an atomization rate of 400 mL/h. The resulting aerosol of the precursor solution was then introduced into a pyrolysis furnace at 600°C. The obtained powder was washed three times with deionized water, dried in an oven at 60°C overnight, and subsequently annealed at 200°C in a H_2/Ar (v/v: 5/95) atmosphere with a heating rate of 1°C/min for 2 h to obtain pristine Cu. pristine Cu was further subjected to Ar plasma treatment for 10 min in an AX-1000 plasma system (13.56 MHz) to obtain low-coordinated Cu (L-Cu).

Electrochemical experiments

Electrochemical experiments were carried out using a commercial flow cell electrolyser (101017, Gaoss Union Technology Co., LTD). A catalyst slurry was prepared by dissolving 25 mg of the catalyst in 3 mL of isopropanol and then adding 20 μL of Nafion ionomer solution (5 wt% in H_2O). Next, the catalyst slurry was slowly dropped onto the carbon paper (Sigracet 29 BC) to attain a catalyst loading of ~0.5 mg cm^{-2} as a gas diffusion electrode (GDE). Nickel mesh was used as the anode

and Ag/AgCl served as the reference electrode. A proton exchange membrane (171001, Nafion N117) was used to separate the cathode and anode chambers. All potentials were referenced to a reversible hydrogen electrode (RHE) by E (V vs. RHE) = E (V vs. Ag/AgCl) + 0.198 V + 0.059 × pH. The catholyte was a solution containing 0.1 M KNO_3 and 0.1 M $KHCO_3$, while the anolyte consisted of a 1 M KOH solution. The catholyte was purged with CO_2 or Ar prior to the electrochemical experiments. During the electrolysis, CO_2 gas was fed from the no-catalyst side of the GDE at a flow rate of 20 s.c.c.m., and both catholyte and anolyte were continuously cycled at a rate of 20 mL min^{-1} under pump drive.

Determination of urea

Urea concentration was detected via urease decomposition method[1]. Typically, 0.2 mL of urease solution with concentration of 5 mg mL^{-1} was added into 2 mL of urea electrolyte, and then reacted at 37℃ in constant temperature shaker for 40 min. Urea was decomposed by urease into CO_2 and two NH_3 molecules. After the decomposition, NH_3 concentration of urea electrolyte with urease (c_{urease}) was detected via above indophenol blue method. Meanwhile, NH_3 concentration contained in urea electrolyte without urease (c_{NH3}) was also quantified by indophenol blue method. Urea concentration (c_{urea}) in electrolyte were calculated by the following equation:

$$c_{urea} = (c_{urease} - c_{NH3})/2 \quad (1)$$

The urea yield rate and FE_{urea} were calculated by the following equation:

$$\text{Urea yield rate } (mmol\ h^{-1}\ cm^{-2}) = \frac{c_{urea} \times V}{60.06 \times t \times A} \quad (2)$$

$$FE_{urea}\ (\%) = \frac{16 \times F \times c_{urea} \times V}{60.06 \times Q} \times 100\% \quad (3)$$

where c_{urea} (mg mL^{-1}) is the measured urea concentration, V (mL) is the volume of the electrolyte, t (h) is the reduction time, A (cm^{-2}) is the surface area of cathode, F (96500 C mol^{-1}) is the Faraday constant, Q (C) is the quantity of applied electricity.

Determination of NH_3

The generated NH_3 was determined by the indophenol blue method[2]. Typically, 2 mL of electrolyte was removed from the electrochemical reaction vessel and diluted with deionized water. Then 2 mL of diluted solution was removed into a clean vessel followed by sequentially adding NaOH solution (2 mL, 1 M) containing $C_7H_6O_3$ (5 wt.%) and $C_6H_5Na_3O_7$ (5 wt.%), NaClO (1 mL, 0.05 M), and $C_5FeN_6Na_2O$ (0.2 mL, 1wt.%) aqueous solution. After the incubation for 2 h at room temperature, the mixed solution was subjected to UV-vis measurement using the absorbance at 655 nm wavelength. The concentration-absorbance curves were calibrated by the standard NH_4Cl solution with a series of concentrations.

Determination of NO_2^-

NO_2^- in electrolyte was determined by a Griess test[3]. Typically, 2 mL of electrolyte was removed from the electrochemical reaction vessel and diluted with deionized water. Coloring solution was prepared by dissolving N-(1-naphthyl) ethylenediamine dihydrochloride (0.1 g), sulfonamide (1.0 g) and H_3PO_4 (2.94 mL, 85%) into 50 ml of deionized water. 0.1 ml coloring solution was added to the diluted electrolyte. After the incubation for 30 min at room temperature, the mixture was subjected to UV-vis measurements and resulted in the absorption spectrum (ranged from 400-700 nm). The absorbance at 540 nm was measured to determine the concentration of generated NO_2^- with a standard curve of $NaNO_2$.

Characterizations

X-ray diffraction (XRD) patterns were obtained using a Rigaku D/max 2400 diffractometer. Transmission electron microscopy (TEM) and high-resolution transmission electron microscopy (HRTEM) were acquired using a Tecnai G2 F20 microscope. Synchrotron radiation based X-ray absorption spectroscopy (XAS) measurements were conducted at the BL14W1 beamline in Shanghai Synchrotron Radiation Facility (SSRF).

Calculation details

DFT calculations were carried out using the Cambridge sequential total energy

package (CASTEP) with ultrasoft pseudopotentials. The exchange-correlation functional is evaluated using the Perdew–Burke–Ernzerhof (PBE) in the generalized gradient approximation. DFT-D3 method was employed to calculate the van der Waals (vdW) interactions. According to the experimental characterizations, pristine Cu has been modeled as 4 × 4 supercell and a vacuum region of 15 Å was used to separate adjacent slabs. Cu (111) slab with removing one surface Cu atom is constructed to simulate L-Cu. The cutoff energy was set as 450 eV and the k-point meshes were set as 3 × 3 × 1.

The computational hydrogen electrode (CHE) model was adopted to calculate the Gibbs free energy change (ΔG) for each elementary step as follows:

$$\Delta G = \Delta E + \Delta E_{ZPE} - T\Delta S \quad (4)$$

where ΔE represents the electronic energy contribution directly derived from DFT calculations. ΔE_{ZPE} and $T\Delta S$ denote the contributions of zero-point energy and entropy (at 298.15 K), respectively. These values can be obtained from the NIST database for free molecules.

Molecular dynamics (MD) simulations were performed using the Forcite module. The electrolyte system was modeled by a cubic cell with placing catalyst at the center of the cell and randomly filling 1000 H_2O, 50 NO_3^-, 20 CO_2 molecules, and 50 H atoms. The force field type was chosen as universal. After geometry optimization, the MD simulations were performed in an NVT ensemble (298 K) with the total simulation time of 5 ns at a time step of 1 fs.

The radial distribution function (RDF) is calculated by:

$$g(r) = \frac{dN}{4\pi\rho r^2 dr} \quad (5)$$

where dN is the amount of molecules in the shell between the central particle r and $r+dr$, ρ is the number density of NO_3^-, CO_2, H_2O and H.

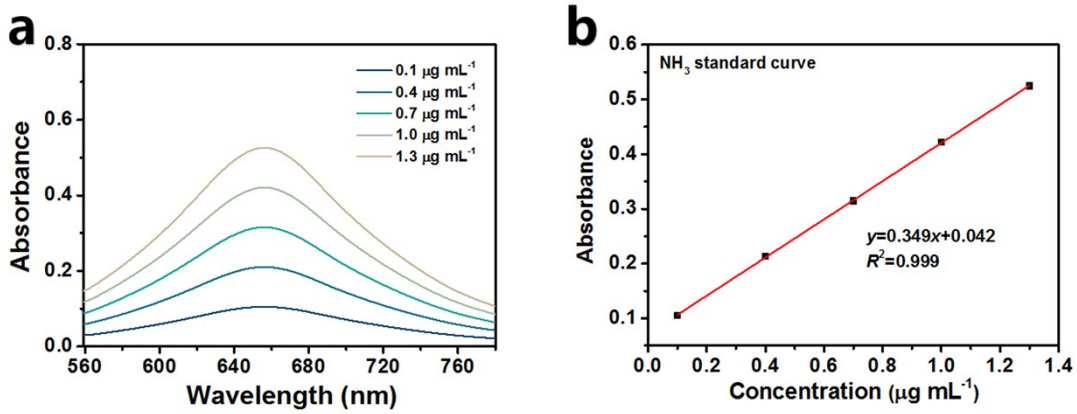

Fig. S1. (a) UV-vis absorption spectra of NH_4Cl assays after incubated for 2 h at ambient conditions. (b) Calibration curve used for the calculation of NH_3 concentrations.

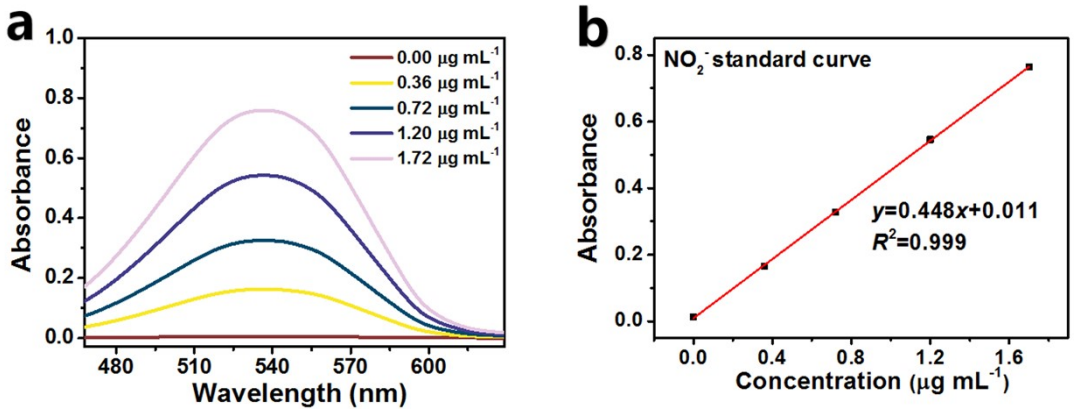

Fig. S2. (a) UV-vis absorption spectra of NO_2^- assays after incubated for 20 min at ambient conditions. (b) Calibration curve used for calculation of NO_2^- concentrations.

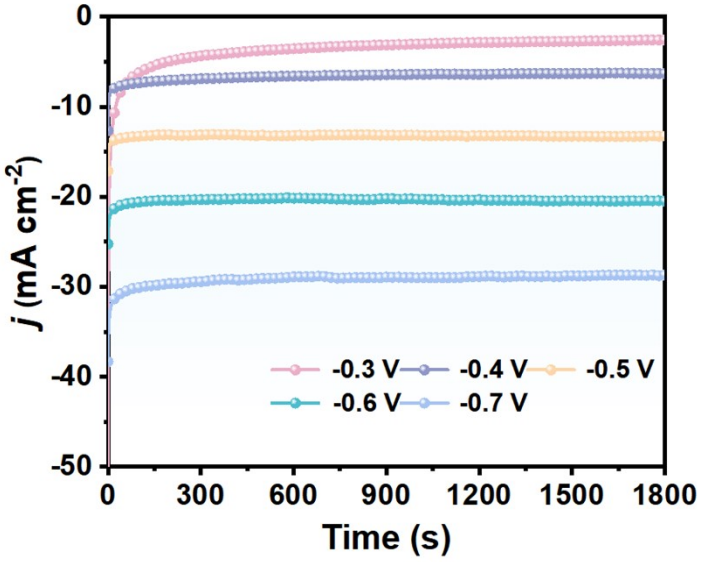

Fig. S3. Chronoamperometry curves of L-Cu at different potentials after 0.5 h of ECNU electrolysis.

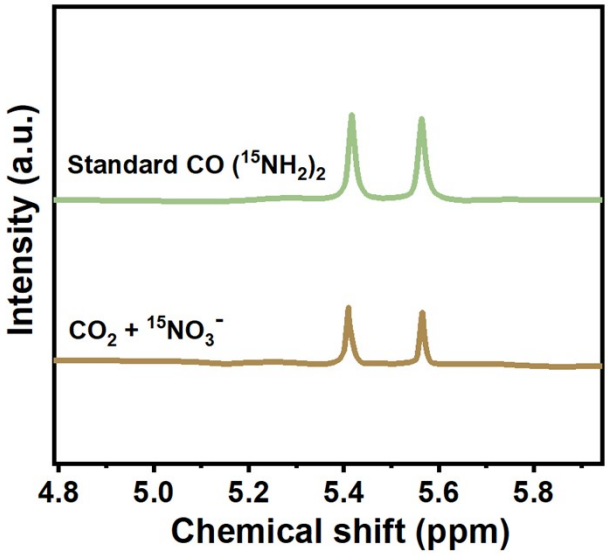

Fig. S4. ^{1}H NMR spectra of CO($^{15}NH_2)_2$ standard sample and those electrolyzed in 0.1 M K$^{15}NO_3$ electrolyte at -0.5 V.

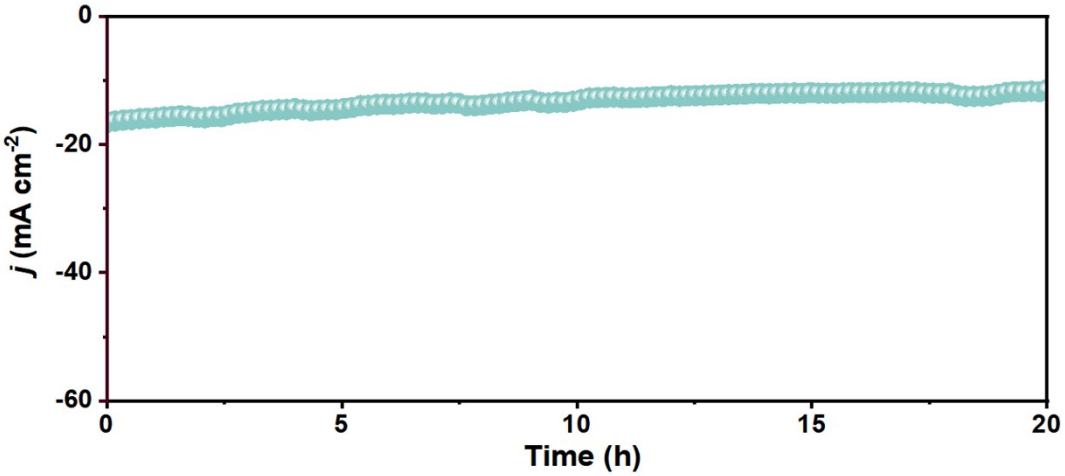

Fig. S5. Long-term stability test of L-Cu for 20 h electrolysis.

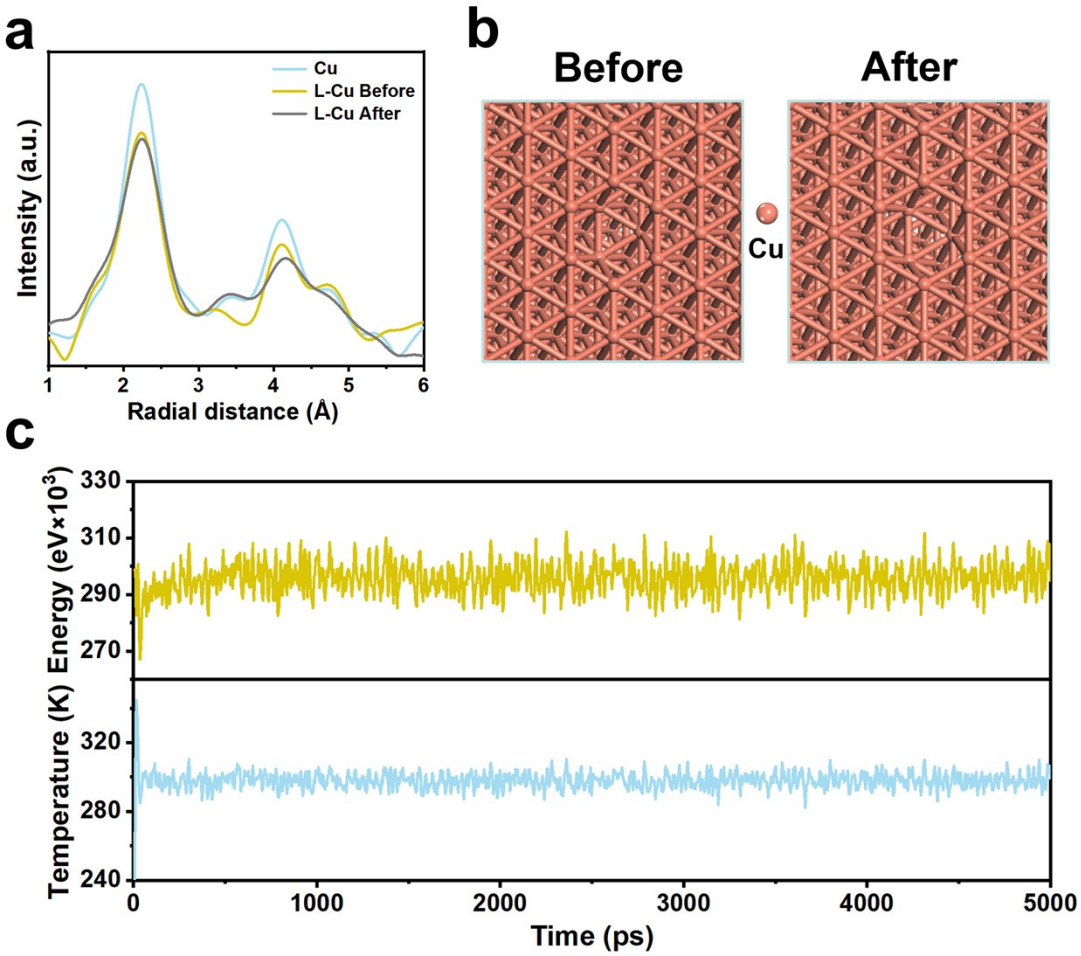

Fig. S6. (a) Cu K-edge EXAFS spectra of L-Cu before and after 1 h ECNU electrolysis at -0.5 V. (b) Geometric structures of L-Cu before and after 5 ns AIMD simulation at 298 K. (c) AIMD simulation of L-Cu atomic structure.

The Cu K-edge EXAFS spectra (Fig. S6a) show that for both Cu and L-Cu, the Cu-Cu bond intensity remains almost the same before and after 1 h ECNU electrolysis at -0.5 V. These results demonstrate that L-Cu maintains the low-coordination sites throughout the ECNU electrolysis. This is attributed to the robust structure of L-Cu (Fig. S6b-c). As shown in Fig. S6b, the original L-Cu configuration retains quite well before and after 5 ns AIMD simulation at 298 K. Meanwhile, the quite stable equilibrium energy/temperature states during 5000 fs of ab initio molecular dynamics (AIMD, Fig. S6c) simulations further prove an exceptional thermodynamic stability of L-Cu. These experimental and theoretical results prove the robust structure of L-Cu with well-retained low-coordination Cu sites during the ECNU electrolysis.

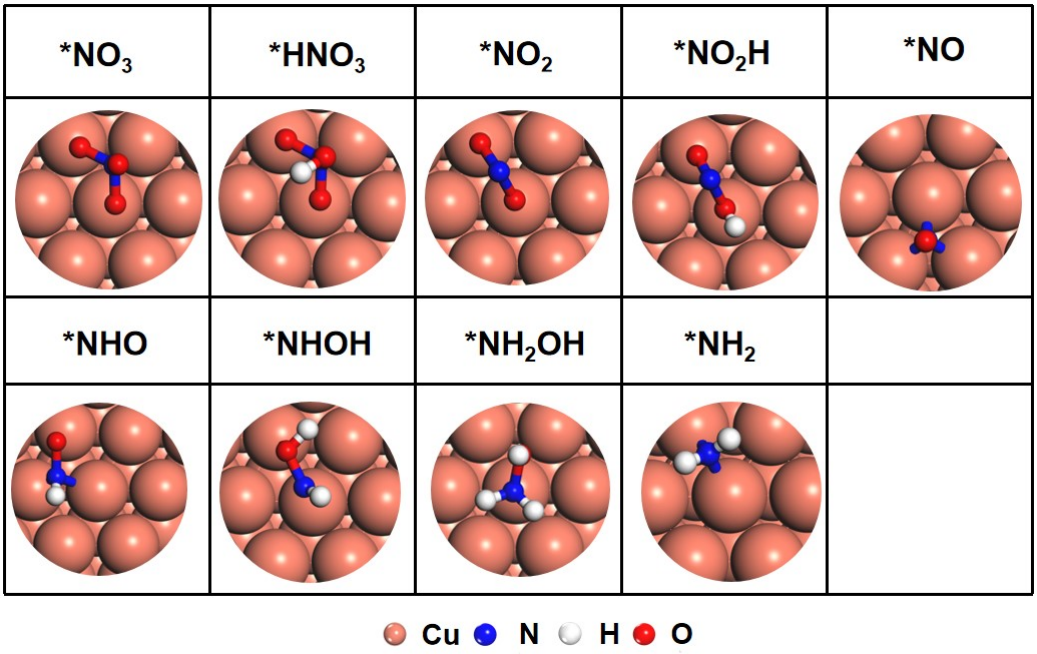

Fig. S7. Optimized atomic configurations of the reaction intermediates on Cu site.

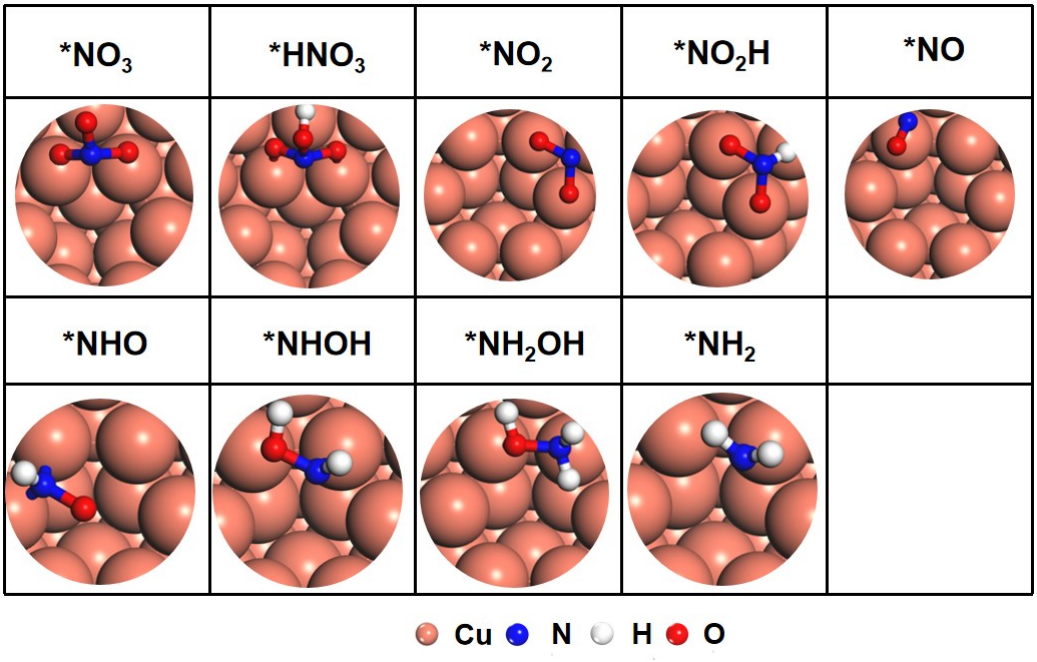

Fig. S8. Optimized atomic configurations of the reaction intermediates on Cu_L site.

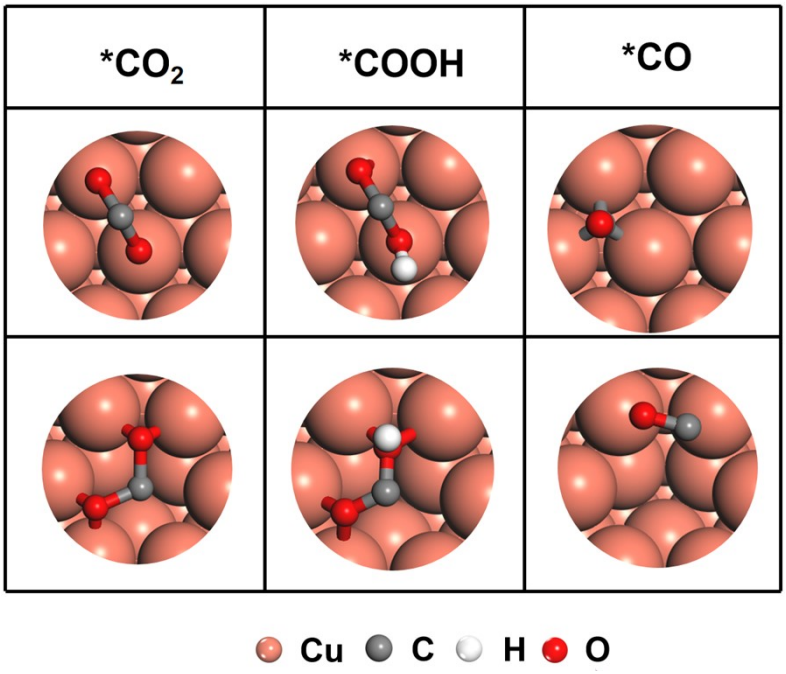

Fig. S9. The intermediate optimized structures of CO_2 → *CO process on Cu site (up) and Cu_L site (bottom).

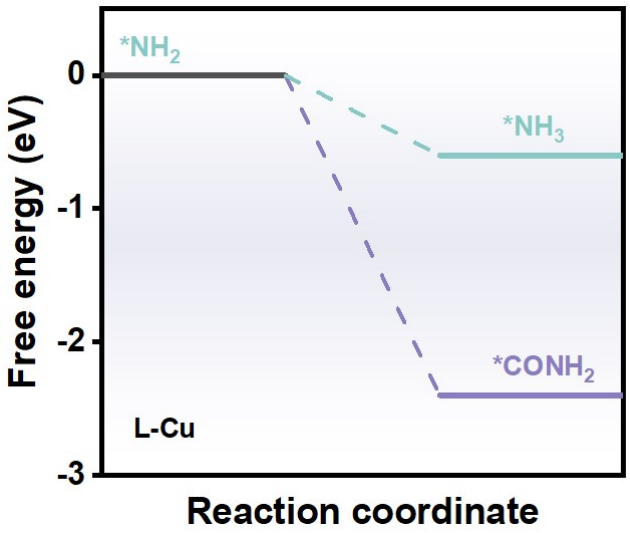

Fig. S10. Free energy diagrams of competition between $*NH_2$-to-$*NH_3$ and $*NH_2$-to-$*CONH_2$.

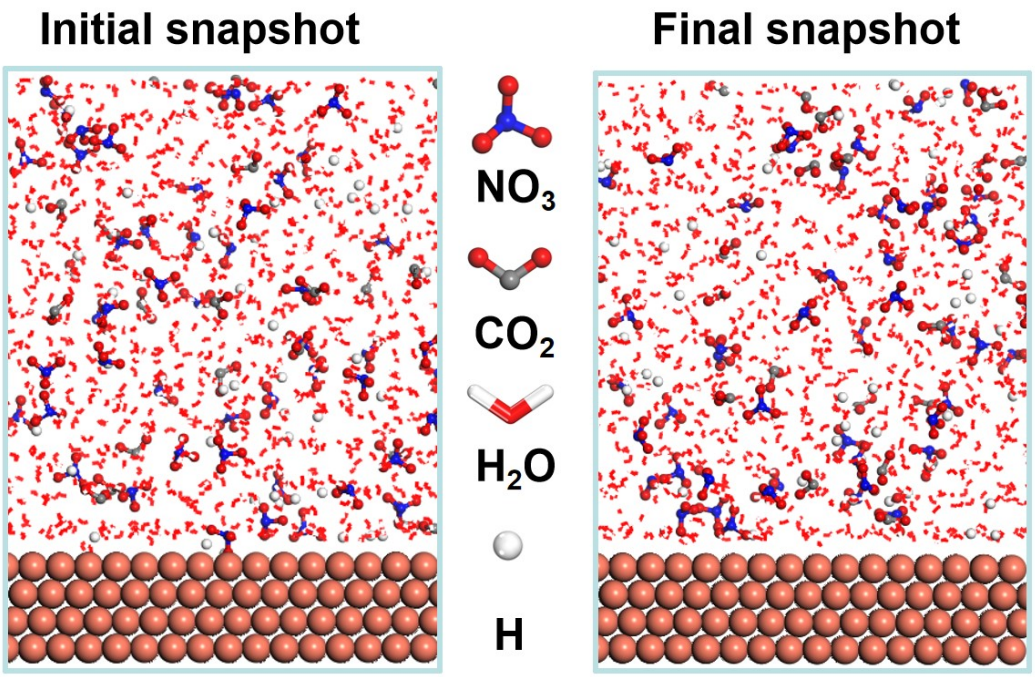

Fig. S11. Initial and final snapshots for the dynamic adsorption process of NO_3^-, CO_2, and H on L-Cu.

Table S1. Comparison of the optimum urea yield rate and FE_{urea} for the recently reported state-of-the-art urea electrocatalysts at ambient conditions.

Catalyst	N/C sources	Electrolyte	Urea yield rate (mmol h^{-1} g^{-1})	FE_{urea} (%)	Potential (V vs. RHE)	Ref.
Vo-S-IO-6	NO_3^-+CO_2	0.1 M KNO_3	15.16	60.6	-0.6	[4]
$In(OH)_3$-S	NO_3^-+CO_2	0.1 M KNO_3	8.88	53.4	-0.6	[5]
MoO_x/C	NO_3^-+CO_2	0.1 M KNO_3	23.83	27.7	-0.6	[6]
$FeNi_3$	NO_3^-+CO_2	0.1 M KNO_3	8.27	16.58	-0.9	[7]
V_O-InOOH	NO_3^-+CO_2	0.1 M KNO_3	9.87	51	-0.5	[8]
Cu-TiO_2-x	NO_2^-+CO_2	0.02 M KNO_2 +0.2 M $KHCO_3$	20.8	43.1	-0.4	[9]
Pd_1-TiO_2	N_2+CO_2	0.1 M KCO_3	2.76	3.79	-0.5	[10]
m-Cu_2O	NO_3^-+CO_2	0.01 M $NaNO_3$ + 0.1 M $KHCO_3$	29.2	9.43	-1.3	[11]
Cu SACs	NO_3^-+CO_2	0.1 M KNO_3 +0.1 M $KHCO_3$	29.97	28	-0.9	[12]
Fe-Ni	NO_3^-+CO_2	0.05 M KNO_3 + 0.1 M $KHCO_3$	20.2	17.8	-1.5	[13]
L-Cu	**NO_3^-+CO_2**	**0.1 M KNO_3 +0.1 M $KHCO_3$**	**30.96**	**50.42**	**-0.5**	**This Work**

Supplementary references

[1]. X. Wei, X. Wen, Y. Liu, C. Chen, C. Xie, D. Wang, M. Qiu, N. He, P. Zhou and W. Chen, *J. Am. Chem. Soc.*, 2022, **144**, 11530-11535.

[2]. P. Li, Z. Jin, Z. Fang and G. Yu, *Energy Environ. Sci.*, 2021, **14**, 3522-3531.

[3]. Z.-Y. Wu, M. Karamad, X. Yong, Q. Huang, D. A. Cullen, P. Zhu, C. Xia, Q. Xiao, M. Shakouri and F.-Y. Chen, *Nat. Commun.*, 2021, **12**, 2870.

[4]. Z. Li, P. Zhou, M. Zhou, H. Jiang, H. Li, S. Liu, H. Zhang, S. Yang and Z. Zhang, *Appl. Catal., B*, 2023, **338**, 122962.

[5]. C. Lv, L. Zhong, H. Liu, Z. Fang, C. Yan, M. Chen, Y. Kong, C. Lee, D. Liu and S. Li, *Nat. Sustain.*, 2021, **4**, 868-876.

[6]. M. Sun, G. Wu, J. Jiang, Y. Yang, A. Du, L. Dai, X. Mao and Q. Qin, *Angew. Chem.*, 2023, **135**, e202301957.

[7]. T. Hou, J. Ding, H. Zhang, S. Chen, Q. Liu, J. Luo and X. Liu, *Mater. Chem. Front.*, 2023, **7**, 4952-4960.

[8]. C. Lv, C. Lee, L. Zhong, H. Liu, J. Liu, L. Yang, C. Yan, W. Yu, H. H. Hng, Z. Qi, L. Song, S. Li, K. P. Loh, Q. Yan and G. Yu, *ACS Nano*, 2022, **16**, 8213-8222.

[9]. N. Cao, Y. Quan, A. Guan, C. Yang, Y. Ji, L. Zhang and G. Zheng, *J. Colloid Interface Sci.*, 2020, **577**, 109-114.

[10]. L. Pan, J. Wang, F. Lu, Q. Liu, Y. Gao, Y. Wang, J. Jiang, C. Sun, J. Wang and X. Wang, *Angew. Chem.*, 2023, **135**, e202216835.

[11]. M. Qiu, X. Zhu, S. Bo, K. Cheng, N. He, K. Gu, D. Song, C. Chen, X. Wei and D. Wang, *CCS Chem.*, 2023, **5**, 2617-2627.

[12]. J. Leverett, T. Tran‐Phu, J. A. Yuwono, P. Kumar, C. Kim, Q. Zhai, C. Han, J. Qu, J. Cairney and A. N. Simonov, *Adv. Energy Mater.*, 2022, **12**, 2201500.

[13]. X. Zhang, X. Zhu, S. Bo, C. Chen, M. Qiu, X. Wei, N. He, C. Xie, W. Chen and J. Zheng, *Nat. Commun.*, 2022, **13**, 5337.